J. Hydrol. Hydromech., 65, 2017, 1, 49–59
DOI: 10.1515/johh-2016-0039

Numerical modelling of two-layer shallow water flow in microtidal salt-wedge estuaries: Finite volume solver and field validation

Nino Krvavica[1], Ivica Kožar[2 *], Vanja Travaš[1], Nevenka Ožanić[1]

[1] Department of Hydrology and Hydraulic Engineering, Faculty of Civil Engineering, University of Rijeka, Radmile Matejčić 3, 51000 Rijeka, Croatia.
[2] Department of Computer Modeling, Faculty of Civil Engineering, University of Rijeka, Radmile Matejčić 3, 51000 Rijeka, Croatia.
* Corresponding author. Tel.: +385 51 265 993. Fax: +385 51 265 998. E-mail: ivica.kozar@uniri.hr

Abstract: A finite volume model for two-layer shallow water flow in microtidal salt-wedge estuaries is presented in this work. The governing equations are a coupled system of shallow water equations with source terms accounting for irregular channel geometry and shear stress at the bed and interface between the layers. To solve this system we applied the Q-scheme of Roe with suitable treatment of source terms, coupling terms, and wet-dry fronts. The proposed numerical model is explicit in time, shock-capturing and it satisfies the extended conservation property for water at rest. The model was validated by comparing the steady-state solutions against a known arrested salt-wedge model and by comparing both steady-state and time-dependant solutions against field observations in Rječina Estuary in Croatia. When the interfacial friction factor λ_i was chosen correctly, the agreement between numerical results and field observations was satisfactory.

Keywords: Finite volume method; Q-schemes; Salt-wedge estuaries; Two-layer flows; Shallow water equations; Rječina Estuary.

INTRODUCTION

Salt-wedge estuaries develop at the mouths of rivers when the ratio of freshwater to tidal flow is large enough to maintain a strong density stratification (Hansen and Rattray Jr, 1966). Under ideal conditions, the vertical profile shows an upper layer of constant salinity equal to zero, separated by a sharp gradient from a lower layer of constant salinity corresponding to seawater. The intensity of interfacial mixing due to tides is reduced by a strong stratification, but a relatively large shear stress is exerted at the interface between the layers. The upper freshwater layer pushes the lower salt-water layer towards the mouth until an equilibrium is achieved between the buoyancy pressure gradient, friction forces, and convective acceleration (Sargent and Jirka, 1987). For steady flow conditions a so called arrested salt-wedge is established, characterized by an active upper layer and a stagnant lower layer.

Schijf and Schönfeld (1953) and Stommel and Farmer (1952) were among first to develop a mathematical theory for representing the dynamics of highly stratified estuaries. Their mathematical models were based on the shallow water equations and the assumption that a salt-wedge can be represented by two-layers of immiscible fluid, divided by a pycnocline of zero thickness. Based on this theory, Schijf and Schönfeld (1953) developed a simple ordinary differential equation (ODE) for computing the shape of arrested salt-wedges (interface depths along the estuary). A number of simplifications are incorporated in this ODE, such as the Boussinesq approximation, no wall or bed shear stress, no mixing, no lower layer dynamics, constant rectangular cross section, and horizontal bottom. In subsequent years, two-layer numerical models for arrested salt-wedges were improved and extended to include wall and bed shear stress (Dermissis and Partheniades, 1985), channel geometry with variable breadth and slope (Balloffet and Borah, 1985), and interfacial mixing (Arita and Jirka, 1987; Grubert, 1989).

Simple two-layer steady-state numerical models are mainly useful for computing the shape of arrested salt wedges, but they can also be used for computing quasi-steady solutions under gradual changes in tides and freshwater discharges. However, in realistic field conditions, steady-states are rarely present due to rather dynamic fluvial and tidal motions. Dazzi and Tomasino (1974) developed a two-layer time-dependent numerical model to study the flow dynamics in a salt-wedge estuary. Even though the main features of tidal flows in Po River have been captured, their model (Dazzi and Tomasino, 1974) neglects the convective acceleration terms in momentum equations. Johnson et al. (1987) developed a laterally averaged estuarine model which was applied to study the salinity intrusion in Mississippi River. This multilayer numerical model includes both convective and diffusive terms in the momentum equation, and it accounts for the temperature and salinity transport between the layers. However, as it was noted by Balloffet and Borah (1985) and Johnson et al. (1987), such models are more appropriate for partially or well mixed estuaries because the numerical diffusion tends to smooth the sharp halocline usually present in salt-wedges. Furthermore, a very fine spatial discretization is needed in 2D and 3D numerical models, especially near the interface, making the practical application of such models questionable due to considerable computational costs. On the other hand, two-layer numerical models can adequately describe all relevant processes in salt-wedge estuaries if the stratification is strong enough to suppress the interfacial mixing, and the thickness of the interfacial layer is much smaller than the thickness of the upper and lower layer. In the past few years, several time-dependant two-layer numerical models (Liu et al., 2015; Ljubenkov, 2015; Sierra et al., 2004) were developed to describe the two-layer flow in salt-wedge estuaries. Although the main features of the stratified flow were captured by these models, they are not shock-capturing, and thus cannot correctly describe the internally transcritical flow which may occur under highly dynamical conditions due to sills or lateral contractions (Armi, 1986, Farmer and Armi, 1986).

Recently, several studies presented and examined shock-capturing numerical models for Shallow Water (SW) flow based on the Finite Volume Method (FVM). A standard Ap-

proximate Riemann Solver can be applied for hyperbolic conservation laws. However, system of equations for SW flow through channels with either sloped bed, variable cross-section width or friction are written as hyperbolic conservation laws with source terms, and standard methods may fail when computing the steady-state solutions (Bermudez and Vázquez-Cendón, 1994). This problem was successfully solved by Bermudez and Vázquez-Cendón (1994) and Vázquez-Cendón (1999) for channels with rectangular cross-sections and variable width, by introducing the Q-scheme and upwinding the source term. The Q-scheme was extended for two-layer flow by Castro et al. (2001) who solved the problem of coupled terms, and further improved by Castro et al. (2004) for channels with variable irregular cross sections. The latter numerical model was verified and validated for exchange flow through channels with simplified geometry by Castro et al. (2004) and successfully applied for the two-layer exchange flow through realistic geometry of Gibraltar Strait (Castro et al., 2007).

Using the techniques presented in (Castro et al., 2004, 2005, 2007; Rebollo et al., 2003) we developed a numerical model for two-layer flow in salt-wedge estuaries with irregular geometry, including shear stress and wet-dry fronts. The considered numerical scheme is based on a generalized Q-scheme of Roe for flux terms and an upwind scheme for source terms accounting for the variable geometry and the shear stress. The model was validated by comparing the numerical results against a two-layer model for arrested salt-wedges (Balloffet and Borah, 1985) in simplified channels with variable bed elevations and a contraction, and by comparing the results against field observations in Rječina Estuary for both steady-states and dynamic flow conditions characterized by a rapid change in freshwater inflow.

METHODOLOGY

In this section we present the governing equations and the numerical scheme for a two-layer shallow water flow in salt-wedge estuaries with irregular geometry, including shear stress and wet-dry transition. We adapted the general formulation for two-layer flows in channels with irregular geometry (Castro et al., 2004). In hydraulic sense, two-layer flows in salt-wedge estuaries are similar to exchange flows in straits or channels, examined recently (Castro et al., 2004, 2007), apart from a few notable differences. First, salt-wedges are under the influence of not one, but a combination of different forcing mechanisms, such as tidal, fluvial, and estuarine (Geyer and Ralston, 2011). The intensity of bed and interfacial shear stress is relatively large in comparison to the exchange-flow. In salt-wedge estuary the upper layer is usually more active than the lower layer which can be motionless or flow in the same or opposite direction. Finally, numerical models for two-layer flows in salt-wedge estuaries almost always include a region inside the spatial domain where a lower layer moving boundary appears. Namely, the tip of a salt-wedge is represented by a lower layer wet-dry front which needs to be adequately resolved.

Governing equations

We consider a two-layer shallow water flow through channels with variable irregular cross sections. Figure 1 shows the schematic longitudinal and cross section of such a channel. The coordinate x refers to the axis of a channel, y is the coordinate normal to the axis, z is the vertical coordinate, and t is time. The freshwater layer of constant density ρ_1 and thickness $h_1(x,t)$ flows over a salt-water layer of constant density ρ_2 and thickness $h_2(x,t)$. The ratio between the upper and lower layer density is denoted by $r = \rho_1/\rho_2$. The flow rate in each layer is defined as $Q_j(x,t) = A_j(x,t)u_j(x,t)$, where $u_j(x,t)$ is horizontal velocity, $A_j(x,t)$ is cross-sectional area, and index $j = 1,2$ refers to the upper and lower layer, respectively. Bed elevation function is defined by $b(x)$, while the breadth function is $\boldsymbol{\sigma}(x,t) = \{\sigma_1(x,t), \sigma_2(x,t), \sigma_3(x,t)\}^T$, where $\sigma_1(x,t)$ is breadth at the free surface, $\sigma_3(x,t)$ is breadth at the interface between the layers, and for σ_2 the following equality holds $1/\sigma_2 = (1-r)/\sigma_3 + r/\sigma_1$.

The governing equations considered here were originally developed by Castro et al. (2004) as a PDE system of two coupled conservation laws with source terms. In addition to the variable geometry, we also consider the bed, wall, and interfacial shear stress. The latter terms are incorporated in the equations similarly as in models for channels with rectangular cross sections (Rebollo et al., 2003). More details in deriving the governing equations, especially the source term accounting for the variable geometry, can be found in (Castro et al., 2004). The governing system of equations in its final form is written as follows

$$\frac{\partial w}{\partial t} + \frac{\partial \mathrm{f}(\boldsymbol{\sigma}, \mathrm{w})}{\partial x} = \mathrm{B}(\boldsymbol{\sigma}, \mathrm{w})\frac{\partial \mathrm{w}}{\partial x} + \mathrm{v}(\boldsymbol{\sigma}, \mathrm{w}) + \mathrm{s}_g(x, \boldsymbol{\sigma}, \mathrm{w}) + \mathrm{s}_f(x, \boldsymbol{\sigma}, \mathrm{w}), \tag{1}$$

where

$$\mathrm{w}(x,t) = \left\{A_1(x,t), Q_1(x,t), A_2(x,t), Q_2(x,t)\right\}^T, \tag{2}$$

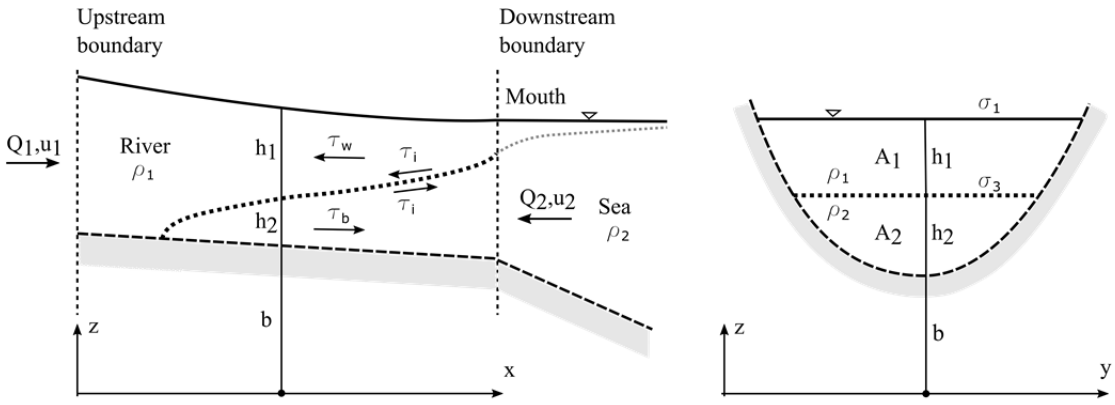

Fig. 1. Characteristic longitudinal and cross section of a salt-wedge.

$$\mathrm{f}(\boldsymbol{\sigma},\mathrm{w})=\begin{Bmatrix} Q_1 \\ \dfrac{Q_1^2}{A_1}+\dfrac{g}{2\sigma_1}A_1^2 \\ Q_2 \\ \dfrac{Q_2^2}{A_2}+\dfrac{g}{2\sigma_2}A_2^2 \end{Bmatrix} \tag{3}$$

$$\mathrm{B}(\boldsymbol{\sigma},\mathrm{w})=\begin{bmatrix} 0 & 0 & 0 & 0 \\ 0 & 0 & -g\dfrac{A_1}{\sigma_1} & 0 \\ 0 & 0 & 0 & 0 \\ -g\dfrac{A_2}{\sigma_1} & 0 & 0 & 0 \end{bmatrix}, \tag{4}$$

$$\mathrm{V}(\boldsymbol{\sigma},\mathrm{w})=\begin{Bmatrix} 0 \\ \dfrac{g}{2}\dfrac{\partial}{\partial x}\left(\dfrac{1}{\sigma_1}\right)A_1^2 \\ 0 \\ \dfrac{g}{2}\dfrac{\partial}{\partial x}\left(\dfrac{1}{\sigma_2}\right)A_2^2 \end{Bmatrix}, \tag{5}$$

The source term s_g accounts for varying geometry

$$\mathrm{S}_g(x,\boldsymbol{\sigma},\mathrm{w})=\begin{Bmatrix} 0 \\ gA_1\left[\dfrac{1}{\sigma_1}\dfrac{\partial}{\partial x}(A_1+A_2)-\dfrac{\partial}{\partial x}(b+h_2+h_1)\right] \\ 0 \\ gA_2\left[\dfrac{1}{\sigma_2}\dfrac{\partial A_2}{\partial x}+\dfrac{r}{\sigma_1}\dfrac{\partial A_1}{\partial x}-\dfrac{\partial}{\partial x}(b+h_2+rh_1)\right] \end{Bmatrix}, \tag{6}$$

while the source term s_f accounts for shear stresses

$$\mathrm{s}_f(x,\boldsymbol{\sigma},\mathrm{w})=\begin{Bmatrix} 0 \\ \dfrac{\tau_w}{\rho_1}O_1'+\dfrac{\tau_i}{\rho_1}\sigma_3 \\ 0 \\ \dfrac{\tau_b}{\rho_2}O_2+\dfrac{\tau_i}{\rho_2}\sigma_3 \end{Bmatrix}, \tag{7}$$

where $O_1' = O_1 - \sigma_3$ and O_2 are upper and lower layer wetted perimeter, respectively. The bed, wall, and interfacial shear stress are defined by Manning's roughness coefficient n or interfacial friction factor λ_i (equal to 1/8 of Darcy-Weisbach factor f), as follows

$$\tau_b=-\rho_2 g n^2 |u_2| u_2 R_2^{-1/3}, \tag{8}$$

$$\tau_w=-\rho_1 g n^2 |u_1| u_1 R_1^{-1/3}, \tag{9}$$

$$\tau_i=-\rho_1\lambda_i |u_1-u_2|(u_1-u_2), \tag{10}$$

where g is gravity acceleration and $R_1 = A_1/O_1'$ and $R_2 = A_2/O_2$ are upper and lower layer hydraulic radius, respectively.

Numerical scheme

To obtain the approximate solution for the system (1) we applied the numerical techniques presented in (Castro et al., 2004). The numerical scheme is explicit in time and based on a Q-scheme of Roe for flux terms and an upwind scheme for source terms. The formal accuracy of the numerical model is first order, although it is second order accurate for steady state solutions (Bermudez and Vázquez-Cendón, 1994). First, the spatial domain is divided into M control volumes or cells $C_i = [x_{i-1/2}, x_{i+1/2}]$, for $i = 1$ to M, where x_i is the centre of the cell, and $x_{i+1/2}$ is the intercell between the cells C_i and C_{i+1}. If we assume that all cells are equal in size, then the cell size can be denoted by $\Delta x = x_{i+1/2} - x_{i-1/2}$, although this method can also be applied for irregular meshes. In general, all variables denoted by the index i refer to values averaged over the cell C_i, and $i + 1/2$ to values at the intercell between cells C_i and C_{i+1}. Also, all variables denoted by index $j = 1$ refer to the upper layer, and by $j = 2$ to the lower layer. The time step is denoted by Δt, and all variables denoted by the upper index n define the value at time $t^n = n\Delta t$. The mesh used for the numerical scheme is shown in Fig. 2.

The Q-scheme for two-layer SW flow through channels with irregular geometry is given in detail in (Castro et al., 2004). However, because the proposed model (Eq. 1) also includes shear stress terms, the main features of the scheme are presented here for completeness and clarity. The following numerical scheme for solving the system (1) is proposed

$$\begin{aligned} \mathrm{w}_i^{n+1} &= \mathrm{w}_i^n + \frac{\Delta t}{\Delta x}\left(\mathrm{f}_{i-1/2}-\mathrm{f}_{i+1/2}\right) \\ &+ \frac{\Delta t}{2\Delta x}\left[\mathrm{B}_{i-1/2}\left(\mathrm{w}_i^n-\mathrm{w}_{i-1}^n\right)+\mathrm{B}_{i+1/2}\left(\mathrm{w}_{i+1}^n-\mathrm{w}_i^n\right)\right] \\ &+ \frac{\Delta t}{2\Delta x}\left(\mathrm{v}_{i-1/2}+\mathrm{v}_{i+1/2}\right)+\frac{\Delta t}{\Delta x}\left(\mathrm{P}_{i-1/2}^{+}\mathrm{s}_{i-1/2}+\mathrm{P}_{i+1/2}^{-}\mathrm{s}_{i+1/2}\right). \end{aligned} \tag{11}$$

The numerical flux at the intercell is defined as

$$\mathrm{f}_{i+1/2}=\frac{1}{2}\left[\mathrm{f}\left(\boldsymbol{\sigma}_i^n,\mathrm{w}_i^n\right)+\mathrm{f}\left(\boldsymbol{\sigma}_{i+1}^n,\mathrm{w}_{i+1}^n\right)\right]-\frac{1}{2}\left|\mathcal{A}_{i+1/2}\right|\left(\mathrm{w}_{i+1}^n-\mathrm{w}_i^n\right), \tag{12}$$

where $\mathcal{A}$ is the numerical viscosity matrix (Castro et al., 2004) defined as

$$\mathcal{A}_{i+1/2}=\mathrm{J}_{i+1/2}-\mathrm{B}_{i+1/2}, \tag{13}$$

and the Jacobian matrix as

$$\mathrm{J}_{i+1/2}=\begin{bmatrix} 0 & 1 & 0 & 0 \\ -u_{i+1/2,1}^2+c_{i+1/2,1}^2 & 2u_{i+1/2,1} & 0 & 0 \\ 0 & 0 & 0 & 1 \\ 0 & 0 & -u_{i+1/2,2}^2+c_{i+1/2,2}^2 & 2u_{i+1/2,2} \end{bmatrix}, \tag{14}$$

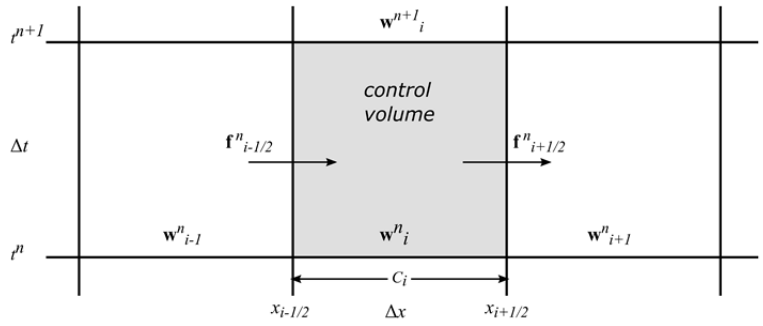

Fig. 2. Finite volume grid scheme, with the updating procedure using an explicit method in time.

with the intermediate values of velocity u and wave speed c computed at intercell $i+1/2$ by the method of Roe (1981)

$$u_{i+1/2,j} = \frac{u_{i,j}\sqrt{A_{i,j}} + u_{i+1,j}\sqrt{A_{i+1,j}}}{\sqrt{A_{i,j}} + \sqrt{A_{i+1,j}}}, \tag{15}$$

$$c_{i+1/2,j} = \sqrt{\frac{g}{\sigma_{i+1/2,j}}\frac{A_{i,j} + A_{i+1,j}}{2}}. \tag{16}$$

$\mathrm{B}_{i+1/2}$ denotes the value of matrix B corresponding to values $\sigma_{i+1/2,j}$ and $A_{i+1/2,j}$.

In order to satisfy the conservation property, the so called C-property (Bermudez and Vázquez-Cendón, 1994),

$$\mathcal{A}_{i+1/2}\left(\mathrm{w}_{i+1} - \mathrm{w}_i\right) = \mathrm{f}\left(\mathrm{w}_{i+1}\right) - \mathrm{f}\left(\mathrm{w}_i\right) - \mathrm{v}_{i+1/2} - \mathrm{B}\left(\mathrm{w}_{i+1} - \mathrm{w}_i\right), \tag{17}$$

vector v must be

$$\mathrm{v}_{i+1/2} = \begin{Bmatrix} 0 \\ v_{i+1/2,1} \\ 0 \\ v_{i+1/2,2} \end{Bmatrix}, \tag{18}$$

where

$$v_{i+1/2,j} = \frac{g}{2}\left(\frac{1}{\sigma_{i+1,j}} - \frac{1}{\sigma_{i+1/2,j}}\right)\left(A_{i+1,j}\right)^2 + \frac{g}{2}\left(\frac{1}{\sigma_{i+1/2,j}} - \frac{1}{\sigma_{i,j}}\right)\left(A_{i,j}\right)^2. \tag{19}$$

The importance of upwinding the source term accounting for bed slope and varying geometry was investigated by Bermudez and Vázquez-Cendón (1994) and Vázquez-Cendón (1999). A similar upwind treatment of friction terms in channels with rectangular cross-sections was proposed by Rebollo et al. (2003). Following these ideas, the projection matrix for upwinding the source term s is defined as

$$\mathrm{P}^{\pm}_{i+1/2} = \frac{1}{2}\mathrm{K}_{i+1/2}\left(\mathrm{Id} \pm \mathrm{sgn}\left(\mathbf{\Lambda}_{i+1/2}\right)\right)\mathrm{K}^{-1}_{i+1/2}, \tag{20}$$

where Id is the identity matrix, $\mathbf{\Lambda}_{i+1/2}$ is the diagonal matrix having as coefficients the eigenvalues of $\mathcal{A}_{i+1/2}$, and by $\mathrm{K}_{i+1/2}$ we denote the matrix whose columns are eigenvectors corresponding to these eigenvalues. Note that the Harten regularization (Harten, 1984) is applied to prevent the numerical viscosity of the Q-scheme from vanishing when any of the eigenvalues of the matrix $\mathcal{A}_{i+1/2}$ becomes equal to zero. The numerical source term s is the sum of s_g (source term accounting for variations in the bed slope and the cross-section area) and s_f (source term accounting for the bed, wall, and interfacial shear stress),

$$\mathrm{s}_{i+1/2} = \begin{Bmatrix} 0 \\ s_{g,i+1/2,(2)} + s_{f,i+1/2,(2)} \\ 0 \\ s_{g,i+1/2,(4)} + s_{f,i+1/2,(4)} \end{Bmatrix}, \tag{21}$$

where

$$s_{g,i+1/2,(2)} = gA_{i+1/2,1}\left[\frac{1}{\sigma_{i+1/2,1}}\left(A_{i+1,1} + A_{i+1,2} - A_{i,1} - A_{i,2}\right) - \left(h_{i+1,1} - h_{i,1} + h_{i+1,2} - h_{i,2} + b_{i+1} - b_i\right)\right], \tag{22}$$

$$s_{g,i+1/2,(4)} = gA_{i+1/2,2}\left[\frac{1}{\sigma_{i+1/2,2}}\left(A_{i+1,2} - A_{i,2}\right) + \frac{r}{\sigma_{i+1/2,1}}\left(A_{i+1,1} - A_{i,1}\right) - \left(h_{i+1,1} - h_{i,1} + r\left(h_{i+1,2} - h_{i,2}\right) + b_{i+1} - b_i\right)\right], \tag{23}$$

and

$$s_{f,i+1/2,(2)} = -gA_{i+1/2,1}\frac{n^2 u_{i+1/2,1}\left|u_{i+1/2,1}\right|}{R^{4/3}_{i+1/2,1}}\Delta x - \lambda_i\left(u_{i+1/2,1} - u_{i+1/2,2}\right)\left|u_{i+1/2,1} - u_{i+1/2,2}\right|\sigma_{i+1/2,3}\Delta x, \tag{24}$$

$$s_{f,i+1/2,(4)} = -gA_{i+1/2,2}\frac{n^2 u_{i+1/2,2}\left|u_{i+1/2,2}\right|}{R^{4/3}_{i+1/2,2}}\Delta x - \lambda_i\left(u_{i+1/2,2} - u_{i+1/2,1}\right)\left|u_{i+1/2,2} - u_{i+1/2,1}\right|\sigma_{i+1/2,3}\Delta x. \tag{25}$$

The explicit numerical schemes are stable only if the spatial step Δx and the temporal step Δt satisfy the Courant-Friedrichs-Lewy (CFL) condition. This condition is implemented in this

work by considering the eigenvalues Λ of the matrix $\mathcal{A}$, so that

$$\max\left(\left|\Lambda_{i+1/2,l}\right|\right)\frac{\Delta t}{\Delta x} \le CFL \le 1, \tag{26}$$

where $1 \le l \le 4$ and $1 \le i \le M$.

Sometimes complex eigenvalues Λ may appear in the matrix $\mathcal{A}$, and the system (1) then loses its hyperbolic character. This problem is related to the occurrence of shear driven instabilities, such as Kelvin-Helmholtz or Holmboe waves. In real flows, these instabilities usually initiate the interfacial mixing which then dissipates some of the turbulent energy. Unfortunately, the considered model is based on two layers of immiscible fluids and cannot simulate unstable flows. However, by adding adequate friction terms, some of the locally confined shear instabilities can be reduces enough to maintain the hyperbolic character of the system. The practical problem is that too much friction can results in excessively diffused results and even produce spurious oscillations in the flow. In Castro et al. (2011) a different strategy for maintaining the hyperbolic character was presented. This numerical workaround is based on the predictor/corrector algorithm, which consists in adding an extra friction term only to those individual cells in which complex eigenvalues are detected at a given time step (Castro et al., 2011). The additional friction should simulate the loss of momentum due to mixing, which is expected in real flows as a result of interfacial instabilities. However, this method is only justified if the occurrence of instabilities is confined in space and time. A more general solution for this problem should consist of a numerical model accounting for both friction and mixing terms, which are variable in space and time and based on a more physical description of the interfacial processes. In the present study and for the examined and presented numerical experiments, no such instabilities were encountered, most probably due to a friction term defined by a calibrated interfacial friction factor, which was adequate enough to maintain the hyperbolic character.

Wet-dry fronts

There are a number of ways to deal with the dry cells (Brufau, 2002; Castro et al., 2005). In this work, we considered a fixed mesh and allowed the control volumes to be wetted by either both layers or by the upper layer alone. To avoid instabilities and negative depths a tolerance parameter ε_{wd} was defined. When $h_{i,2} < \varepsilon_{wd}$ the cell C_i is considered to be wetted only by the upper layer; lower layer velocity is set to zero $u_{i,2} = 0$, but the depth $h_{i,2}$ remains unchanged in order to preserve the mass conservation property of the scheme. Note that the value of ε_{wd} should be chosen as small as possible for more accurate results.

It is said that the treatment of wet-dry fronts is considered appropriate if the numerical scheme satisfies the extended C-property (Castro et al., 2005). This condition implies that a numerical steady-state solution for water at rest including wet-dry fronts has to exactly conserve the mass and momentum equations, without any spurious oscillations. Otherwise, dry cells may become artificial wetted, and non-physical flow may appear. Brufau (2002) presented a numerical scheme for one-layer flow satisfying the C-property. An extension for two-layer flow through channels with rectangular cross-sections was derived by Castro et al. (2005). This two-layer scheme, adapted for a more general case of channels with irregular cross sections, is presented here to resolve the wet-dry fronts.

We considered the case when only the lower layer disappears, although a similar condition can be applied for the disappearance of both layers. If function $b(x)$ is regular enough, and assuming a constant bed elevation in each cell, with discontinuities at the cell interfaces, we need to redefine the numerical source term for bed elevation and set appropriate reflection conditions. For the wet-dry transition occurring at the interface $i + 1/2$, between the cells C_i and C_{i+1}, the lower layer source term (Eq. 23) is modified by redefining the part of the source term accounting for the bed elevations, $\Delta b = b_{i+1} - b_i$, as

$$\Delta b = \begin{cases} r\left(b_{i+1} - b_i\right) + (1-r)h_{i,2} & \text{if} \quad h_{i+1,2} < \varepsilon_{wd} \quad \text{and} \quad h_{i,2} \le \Delta b \\ r\left(b_{i+1} - b_i\right) - (1-r)h_{i+1,2} & \text{if } h_{i,2} < \varepsilon_{wd} \text{ and } h_{i+1,2} \le -\Delta b \\ b_{i+1} - b_i & \text{otherwise} \end{cases}. \tag{27}$$

Furthermore, under general assumption that the cell C_i is wetted only by the upper layer ($h_{i,2} < \varepsilon_{wd}$), we also impose the reflection conditions which ensure that the wet-dry front is not allowed to advance until the lower layer depth $h_{i,2}$ becomes larger than the bed step Δb (Fig. 3). If the flow rate in the entire wetted cell is set to zero, the advancement of wet-dry fronts may not be correctly simulated (Castro et al., 2005). To improve the treatment of wet-dry fronts, Castro et al. (2005) proposed that only the flow rate at the intercell $Q_{i+1/2,2}$ is set to zero, while $Q_{i,2}$ in the wetted cell can be computed by Eq. (11). This condition is written here as follows,

$$Q_{i+1/2,2} = \begin{cases} 0 & \text{if} \quad h_{i+1,2} < \varepsilon_{wd} \quad \text{and} \quad h_{i,2} \le \Delta b \\ 0 & \text{if} \quad h_{i,2} < \varepsilon_{wd} \quad \text{and} \quad h_{i+1,2} \le -\Delta b \\ A_{i+1/2,2} u_{i+1/2,2} & \text{otherwise} \end{cases}. \tag{28}$$

Clearly, the smaller ε_{wd} and $Q_{i+1/2,2}$ are, the better this approximation should be.

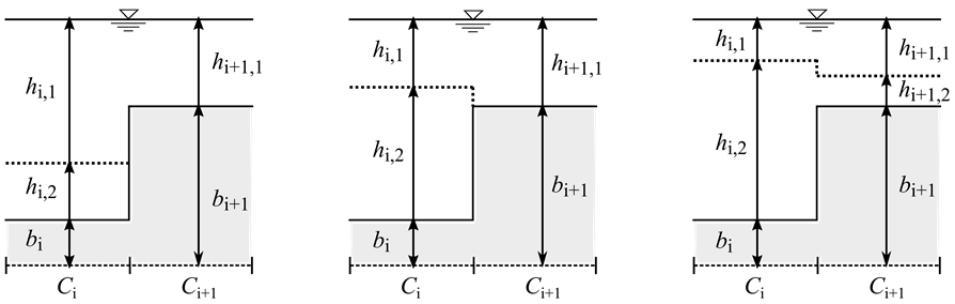

Fig. 3. Wet-dry fronts, left: bed elevation redefinition and reflective condition is needed, middle and right: no redefinition needed.

However, the problem of wetting and drying in two-layer flows is still not completely resolved, especially if high accuracy in computing the propagation velocity of wet-dry fronts is required. Recently, a more physically accurate treatment was proposed by Castro et al. (2006) in which a nonlinear Riemann problem is solved at all intercells where a wet-dry front is detected. Unfortunately, this numerical treatment is not easily extended to a two-layer case (Castro et al., 2006). Besides, the maximum differences in propagation velocities of the wet-dry front for a single layer, between the treatment by Castro et al. (2005) and the more advanced treatment solving nonlinear Riemann problem, was under 5% for all experiments presented by Castro et al. (2006). This difference in accuracy can be considered minimal for field application.

Boundary condition

In arrested salt-wedge models, it is usually assumed that the flow in the upper layer is critical at the mouth (Balloffet and Borah, 1985; Schijf and Schonfeld, 1953). This is true for arrested salt-wedges in prismatic channels with abrupt transitions to the open sea. However, in time-dependant models both layers are active and the critical flow should be described by a composite Froude number G as

$$G^2 \cong F_1^2 + F_2^2 = 1, \tag{29}$$

$$\text{with } F_1^2 = \frac{Q_1^2 \sigma_1}{g(1-r)A_1^3}\frac{\sigma_3}{\sigma_2} \quad \text{and} \quad F_2^2 = \frac{Q_2^2 \sigma_3}{g(1-r)A_2^3}, \tag{30}$$

where F_1 and F_2 are internal Froude numbers for the upper and lower layer, respectively, when irregular cross sections are considered (Castro et al., 2004). The Eq. (29) is solved iteratively for known values of flow rate (Q_1, Q_2), and unknown values of cross-section area (A_1, A_2) and breath (σ_1, σ_1 and σ_1), which are functions of upper layer depth h_1 and total depth $H = h_1 + h_2$. Sometimes, it is difficult to determine the exact position of the mouth for the realistic geometry of the salt-wedge estuaries. However, Armi (1986) showed that in two-layer flows an internally critical flow (hydraulic control point) may also be located at a point where strong lateral contractions are present, which are more easily identified.

NUMERICAL RESULTS

In this section we present several numerical experiments to validate and asses the performance of the proposed model. First, we consider a simplified channel with variable bed elevations and a lateral contraction. The model was applied to compute the shape of an arrested salt-wedge in this channel. Next, a realistic geometry of Rječina Estuary is considered, based on a series of measured cross sections in the field. The model was applied again to compute the arrested salt-wedge, and the results were compared to the field observations. Finally, a numerical experiment is presented in which we examined the dynamic response of the salt-wedge in Rječina Estuary during a freshwater inflow decrease. Both the computed interface depths along the wedge and flow rates per unit width, near the river mouth, were compared against field observations.

In all three sets of experiments we used a relatively small spatial step $\Delta x = 10$ m to account for all changes in the channel geometry, and a fixed time step $\Delta t = 0.5$ s. Depending on the eigenvalue of the matrix $\mathcal{A}$, the CFL number varied during the simulation; it showed a mean value around 0.5 and always remained below 1.0, which is an upper boundary for stability (Eq. 26). Since explicit numerical schemes are known to become more diffusive for lower CFL number, we tested several time steps corresponding to the mean CFL values ranging from 0.2 to 0.8 and found only minor differences in the numerical solutions ($max|h_{CFL=0.2} - h_{CFL=0.8}| < 10^{-3}$).

Arrested salt-wedge in a channel with variable bed elevations and a contraction

The goal of this numerical experiment is to verify the ability of the model to correctly compute steady-state solutions of an arrested salt-wedge in a simplified channel with variable bed elevations and a lateral contraction. Several numerical solutions were compared against the results obtained by a two-layer arrested salt-wedge model (ASWM), developed by Balloffet and Borah (1985), for given flow parameters and boundary conditions.

The geometry of 1000 m long channel is defined by the following bed elevation function (Fig. 4a)

$$b(x) = \frac{2.3}{cosh^2(x/600)} \tag{31}$$

and rectangular cross-sections with a contraction located at middle of the channel (Fig. 4b)

$$\sigma(x) = 20 + 10\left(1 - e^{-9(x/500-1)^2}\right). \tag{32}$$

The 1000 m long channel was represented by $M = 100$ cells. Figure 5a shows the initial condition; the two layers are divided by a horizontal interface located at half way between the surface and the channel bed. The density ratio was set to $r = 0.9756$, corresponding to freshwater density $\rho_1 = 1000$ kg m^{-3} and saltwater density $\rho_2 = 1025$ kg m^{-3}. The bed and wall friction were defined by Manning's roughness coefficient $n = 0.025$ m$^{-1/3}$ s and interfacial friction $\lambda_i = 1 \cdot 10^{-3}$. Downstream boundary conditions were defined by the Eq. (29) and a constant total depth $h_1(t, x_M) + h_2(t, x_M) = const$. At the upstream boundary, a freshwater flow rate was defined as constant in time and equal to the initial flow rate $Q_1(t, 0) = Q_1(0,0)$. The numerical experiment was repeated for five scenarios by varying the freshwater flow rate: a) $Q_1 = 4$ m^{3}s^{-1}, b) $Q_1 = 6$ m^{3}s^{-1}, c) $Q_1 = 9$ m^{3}s^{-1}, d) $Q_1 = 13$ m^{3}s^{-1}, e) $Q_1 = 18$ m^{3}s^{-1}. The simulation ended when a steady-state was reached $\frac{dQ_1}{dt} = 0$.

Figure 5 shows the initial condition and five computed steady-state solutions from the proposed model compared against the results obtained by an arrested salt-wedge model (Balloffet and Borah, 1985). The agreement between two models is satisfactory for all five cases. The influence of the channel contraction is noticeable in all examples as a local shape deformation of the interface line (Figure 5b–f).

Application to Rječina Estuary: arrested salt-wedge

In this numerical experiment we computed several steady-state solutions of an arrested salt-wedge in channel with realistic geometry. To validate the proposed numerical model, we compared the results against observed interface depths along the Rječina Estuary. Furthermore, steady-state solutions were also used as initial conditions for the simulation of the dynamic response of the salt-wedge, presented in the next section.

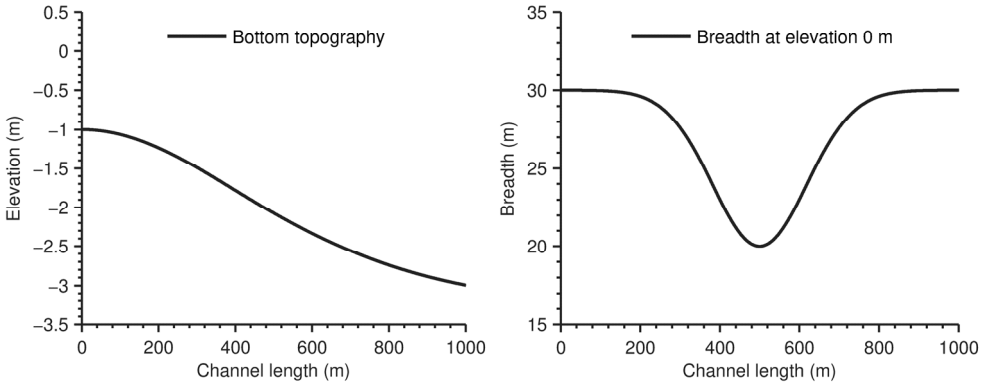

a) bottom topograhpy b) breadth variations

Fig. 4. Channel bottom topography and breadth variations.

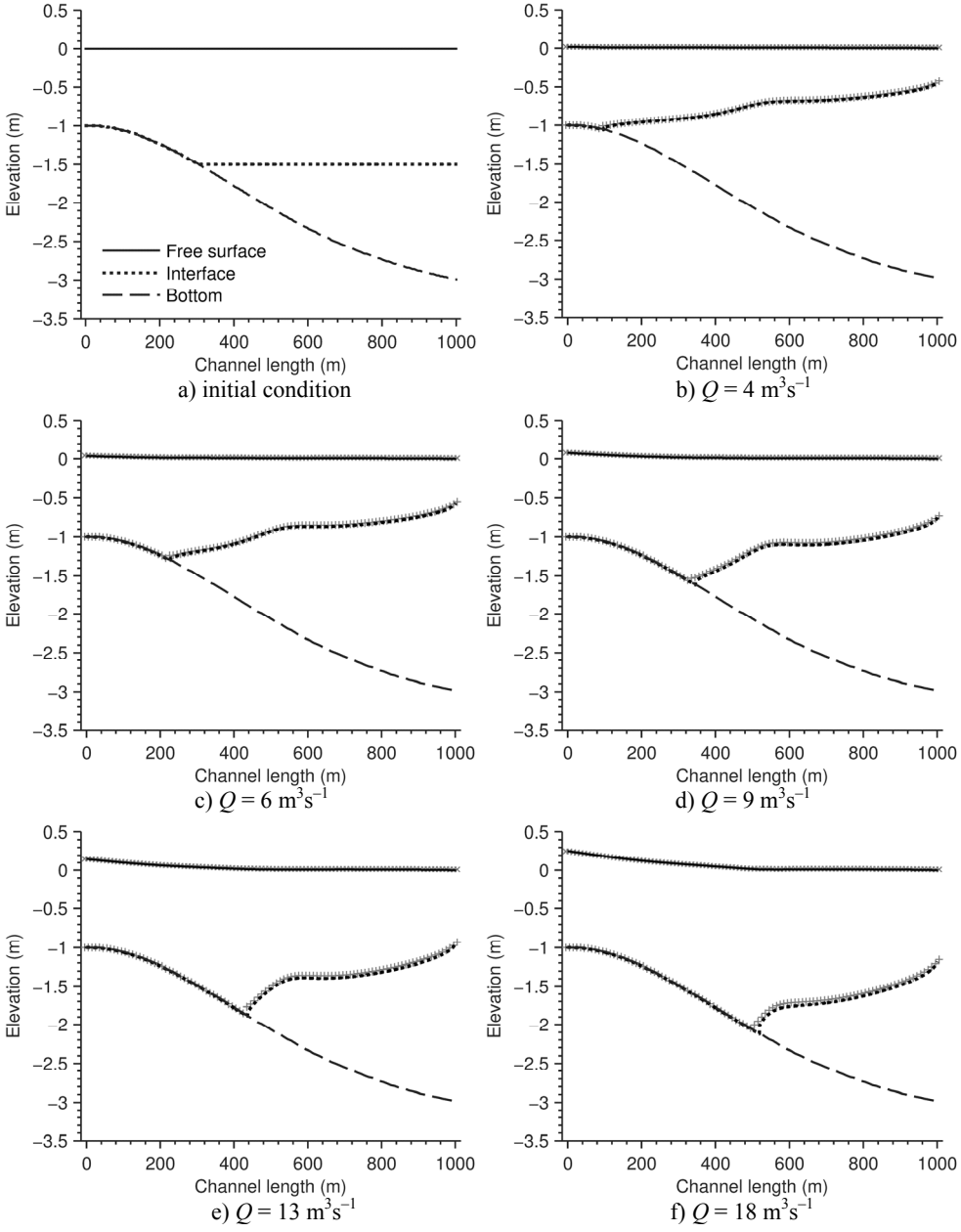

a) initial condition b) $Q = 4\ m^3s^{-1}$

c) $Q = 6\ m^3s^{-1}$ d) $Q = 9\ m^3s^{-1}$

e) $Q = 13\ m^3s^{-1}$ f) $Q = 18\ m^3s^{-1}$

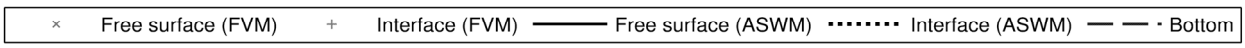

Fig. 5. Initial conditions and comparison of steady-state solutions from the proposed numerical model and arrested salt-wedge model (ASWM), for different freshwater discharges.

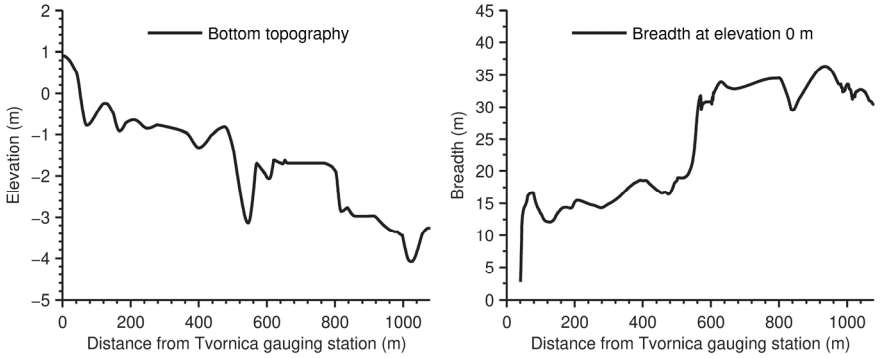

a) bottom topography b) breadth variations

Fig. 6. Bottom topography and breadth variations in Rječina Estuary.

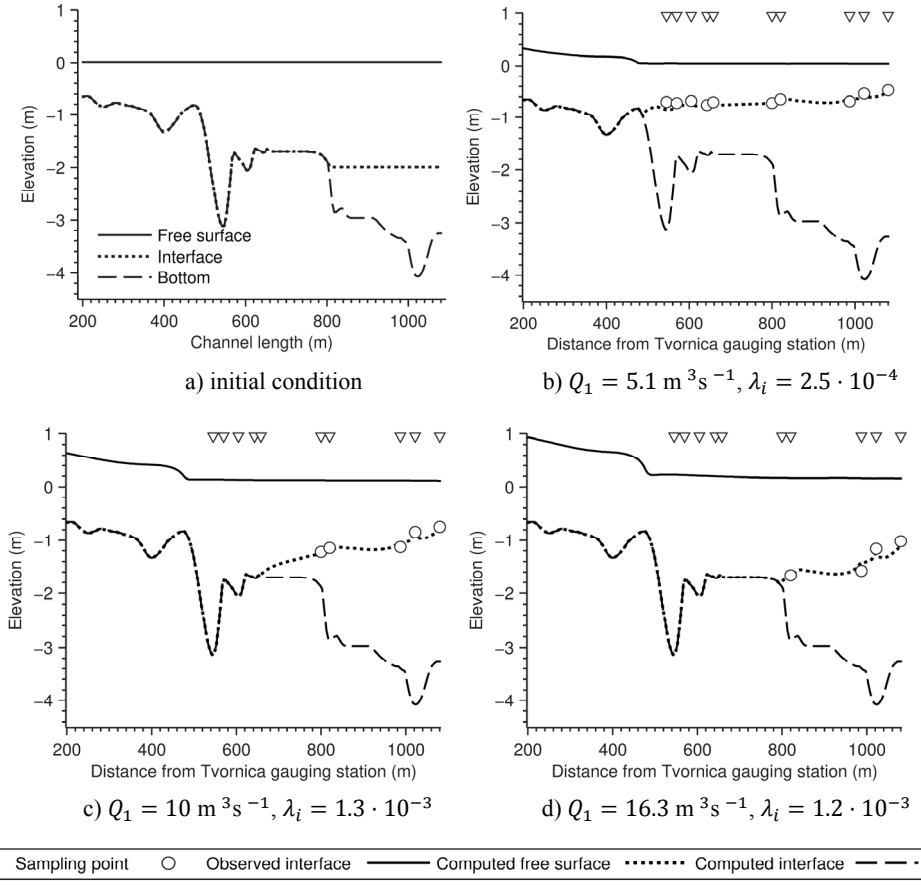

a) initial condition b) $Q_1 = 5.1\ \mathrm{m}^3\mathrm{s}^{-1}$, $\lambda_i = 2.5 \cdot 10^{-4}$

c) $Q_1 = 10\ \mathrm{m}^3\mathrm{s}^{-1}$, $\lambda_i = 1.3 \cdot 10^{-3}$ d) $Q_1 = 16.3\ \mathrm{m}^3\mathrm{s}^{-1}$, $\lambda_i = 1.2 \cdot 10^{-3}$

Fig. 7. Initial conditions and a comparison of steady-state solutions and field observations in Rječina.

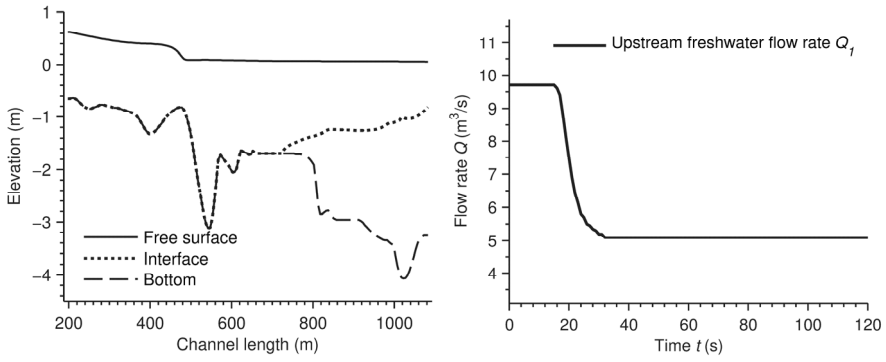

a) initial conditions b) upstream boundary condition

Fig. 8. Initial condition and upstream boundary condition at Rječina Estuary.

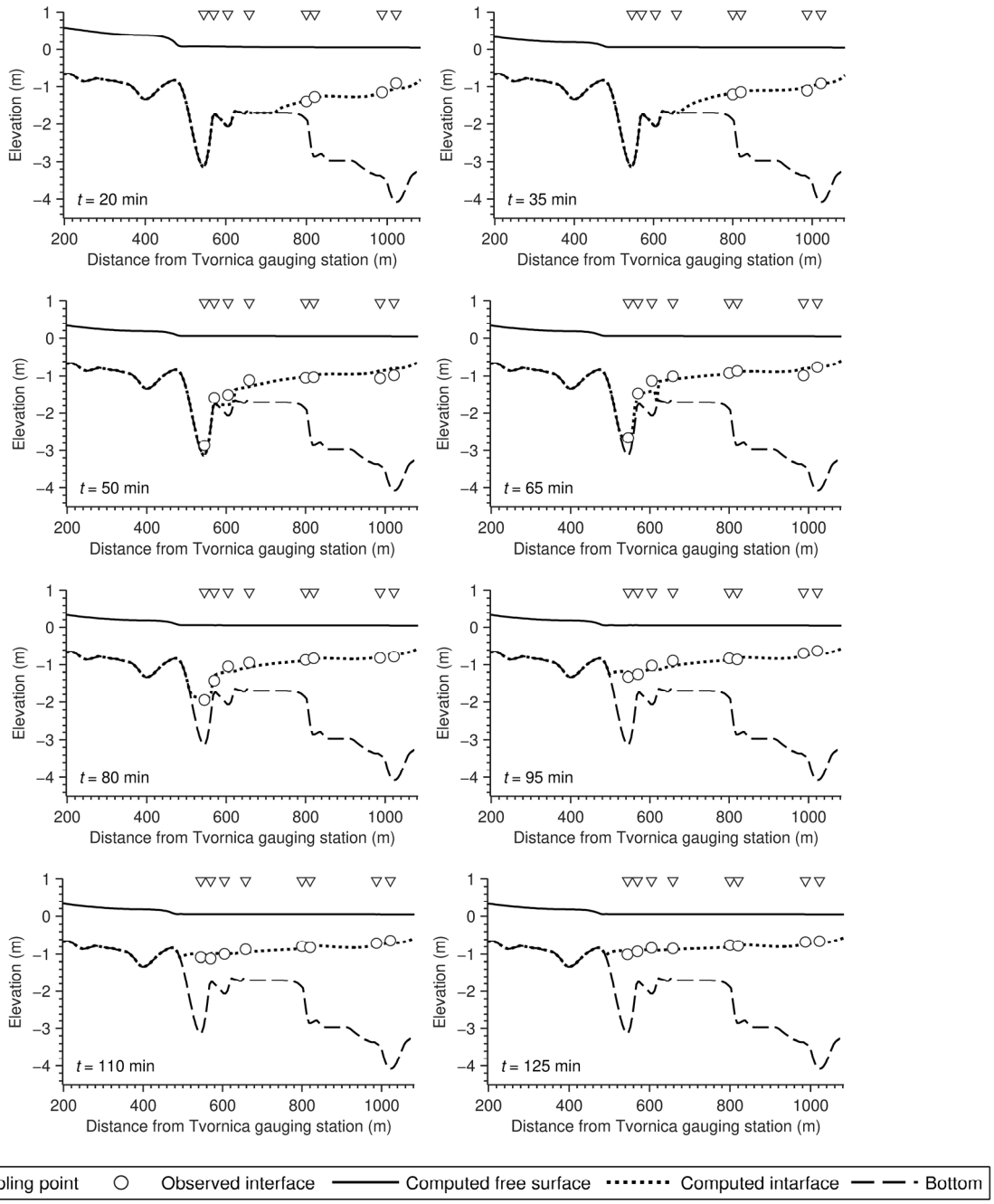

Fig. 9. The intrusion of a salt-wedge in Rječina Estuary during a freshwater inflow decrease (comparison of numerical results and field observations).

The channel bottom topography and breadth variations at the surface are shown in Fig. 6. The 1080 m long channel was represented by $M = 108$ cells. The upstream boundary is placed near the gauging station Tvornica, which is outside the influence of the salt-wedge intrusion. The downstream boundary is placed at the last bridge near the mouth, located at a distance of 1080 m from the gauging station. Krvavica et al. (2012) examined the hydraulic conditions in Rječina Estuary, and found that the hydraulic control point is located at the last bridge, for all riverine and tidal conditions considered here. Krvavica et al. (2012) also showed that the arrested salt-wedge is frequently formed in Rječina Estuary because of the microtidal environment, controlled freshwater discharge, and its relatively short intrusion length. Figure 7a shows the initial condition; two layers are divided by a horizontal interface located between the surface and the channel bed. The density ratio was set to $r = 0.9756$, corresponding to freshwater density $\rho_1 = 1000$ kg m^{-3} and salt-water density $\rho_2 = 1025$ kg m^{-3}. The bed and wall friction were defined by n =0.025 m$^{-1/3}$s, and λ_i was determined by fitting the results to the observed data. Downstream boundary conditions were defined by the Eq. (29) and a constant total depth $h_1(t, x_M) + h_2(t, x_M) = const$. At the upstream boundary a freshwater flow rate was defined as constant in time and equal to the initial flow rate $Q_1(t, 0) = Q_1(0,0)$. The following cases were examined: a) $Q_1 = 5.1$ m^{3}s^{-1}, $\lambda_i = 2.5 \cdot 10^{-4}$, b) $Q_1 = 10$ m^{3}s^{-1}, $\lambda_i = 1.3 \cdot 10^{-3}$, c) $Q_1 = 16.3$ m^{3}s^{-1}, $\lambda_i = 1.2 \cdot 10^{-3}$. The simulation ended when a steady state was reached $\frac{dQ_1}{dt} = 0$.

Figure 7 shows the initial condition and three steady-state solutions reached by the proposed numerical model compared to field observations. In general, for higher freshwater discharges Q_1 the arrested salt-wedge is shorter and the interface is position lower. The variable slope of the interface is the result of variable geometry. These findings confirm the importance of using a model for variable irregular geometry, when the exact shape of the interface is required. The shape and intrusion length of the arrested salt-wedge depends greatly on the interfacial friction factor λ_i, which increases with freshwater flow. When λ_i was calibrated, the agreement between numerical results and field observations was satisfactory.

Application to Rječina Estuary: salt-wedge dynamics

In this final experiment, we assessed the model performance in simulating the dynamic response of a salt-wedge in irregular channel geometry under variable freshwater flow rate. For that purpose, we observed the dynamics of a salt-wedge in Rječina Estuary before, during, and after the freshwater flow rate decrease. The observed interface depths h_j and flow rates per unit width $q_j = h_j u_j$, $j = 1,2$, near the mouth, were compared with the numerical results

As in the previous case, the channel bottom topography and breadth variations at the surface are shown in Fig. 8. The 1080 m long channel was represented by $M = 108$ cells. The upstream and downstream boundary were placed at the same locations as in the previous case (gauging station Tvornica and the last bridge near the mouth). The initial condition was obtained from a steady-state solution presented in the previous section (Fig. 8a). The density ratio was set to $r = 0.9756$, corresponding to freshwater density $\rho_1 = 1000$ kg m^{-3} and salt-water density $\rho_2 = 1025$ kg m^{-3}. The bed and wall friction were defined by $n = 0.025$ m$^{-1/3}$s, and the interfacial friction factor was reduced during the simulation from $\lambda_i = 1.8 \cdot 10^{-3}$ to $\lambda_i = 0.5 \cdot 10^{-3}$ in 17 min, to correspond to a decrease in the freshwater flow rate. Downstream boundary conditions were defined by the Eq. (29) and a constant total depth $h_1(t, x_M) + h_2(t, x_M) = const$. The flow rate at the upstream boundary corresponds to the observed values; freshwater flow was initially set to $Q_1 = 9.7$ m^{3}s^{-1} and it decreased to $Q_1 = 5.1$ m^{3}s^{-1} in 17 min (Fig. 8b). The total simulation time was 125 min.

Figure 9 shows the computed and observed interface depths along the wedge for several time steps. As the freshwater flow Q_1 decreases the salt-wedge advances upstream. The rate at which the salt-wedge is intruding upstream was captured quite well by the numerical model (Fig. 9). The computed values of the flow rate per unit width q_j also agree very well with the observed values (Fig. 10). The only difference is noticeable for the upper layer q_1 during a short period immediately after the inflow decrease has started. It seems that the salt-wedge response to the change in the freshwater inflow was faster than the model has predicted. This difference could be explained by the first-order accuracy of the numerical scheme, which is known to be more diffusive than higher-order methods. Another explanation could be found in the interfacial instabilities and intensified mixing near the mouth, which cannot be accurately captured by this model. However, the overall agreement in the shape of the salt-wedge and flow rates near the mouth is surprisingly good, especially considering all of the simplifications included in this model, such as one-dimensional structure, only two-layers, and no mixing between the layers.

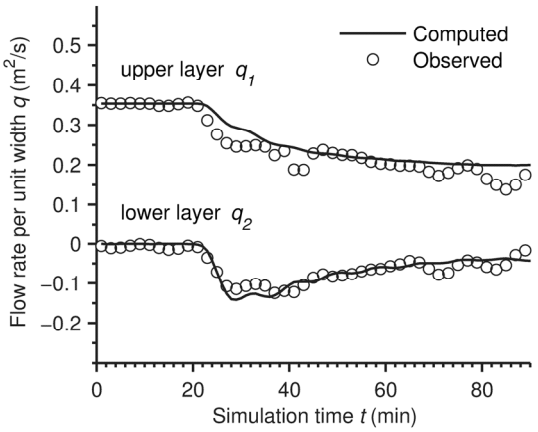

Fig. 10. Comparison of computed and observed flow rates per unit width near the mouth, in the upper q_1 and lower layer q_2, during a freshwater inflow decrease in Rječina Estuary.

CONCLUSIONS

In this work, we presented a one-dimensional shock-capturing finite volume model for salt-wedge estuaries with irregular geometry. We adapted the general formulation for two-layer flow in channels with irregular geometry and the numerical model based on a Q-scheme of Roe (Castro et al., 2004). We additionally included the bed and interfacial shear stress, derived a suitable treatment for the lower layer wet-dry fronts in irregular channels, and defined an appropriate downstream boundary condition.

The model performance was validated by comparing the numerical results against a known steady-state model (Balloffet and Borah, 1985) for the arrested salt-wedge in a simplified channel with variable bed elevations and a contraction. The steady-state solutions were properly simulated by the proposed model for all considered cases. We also assessed the model performance in computing the shape of an arrested salt-wedge in a realistic channel geometry. For that purpose, the steady-state solutions were compared against the field observations in Rječina Estuary, and the agreement was very good for all analysed flow conditions. However, the computed shape of an arrested salt-wedge depends strongly on interfacial friction factor λ_i and the agreement was satisfactory only when λ_i was calibrated. Finally, we assessed the model performance in simulating the dynamic response of a salt-wedge in Rječina Estuary to a freshwater inflow decrease. We used the steady-state solution as initial condition. The agreement between the computed solutions at every time step was very good when compared against field measurements, in both the shape of salt-wedge and flow rates in the upper and lower layer.

Although we used a simple one-dimensional model, these findings confirm that the proposed model can accurately capture the shape of an arrested salt-wedge in irregular geometry and compute the rate of salt-water intrusion. We used a first order numerical scheme combined with relatively dense mesh; if more accurate results are required or wider mesh is preferred, the numerical scheme can easily be extended to higher order schemes, as for example in Castro et al. (2009a) or Castro et al. (2009b). When the interfacial friction factor is chosen appropriately, the model can be used to examine the complex dynamic processes occurring in realistic salt-wedge estuaries, such as Rječina Estuary. We plan to further extend this model by including the process of interfacial mixing which will improve the accuracy of the model, as well as resolve possible issues of

unstable flow occurrence. This improvement will possibly include a third interfacial layer to more accurately simulate the flow when a strong stratification in salt-wedge estuary is compromised.

Acknowledgements. This work has been supported in part by Ministry of Science, Education and Sports of the Republic of Croatia under the project Hydrology of Sensitive Water Resources in Karst (114-0982709-2549) and Research Infrastructure for Campus-based Laboratories at the University of Rijeka (RC.2.2.06-0001), which was co-funded from the European Fund for Regional Development. The support was also given in part by the University of Rijeka under the project Hydrology of Water Resources and Risk Identification from Floods and Mudflows in Karst Areas (13.05.1.1.03) and Experimental Research of Saltwater and Fresh Water Interaction at the Lower Reaches of Rječina River and at the Rječina Estuary (13.05.2.2.14).

REFERENCES

Arita, M., Jirka, G.H., 1987. Two-layer model of saline wedge. II: Prediction. J. Hydraul. Eng., 113, 10, 1249–1263.

Armi, L., 1986. The hydraulics of two flowing layers with different densities. J. Fluid Mech., 163, 27–58.

Balloffet, A., Borah, D.K., 1985. Lower Mississippi Salinity Analysis. J. Hydraul. Eng., 111, 2, 300–315.

Bermudez, A., Vázquez-Cendón, M., 1994. Upwind methods for hyperbolic conservation laws with source terms. Comput. Fluids, 23, 8, 1049–1071.

Brufau, P., 2002. A numerical model for the flooding and drying of irregular domains. Int. J. Numer. Methods Fluids, 39, 3, 247–275.

Castro, M.J., Macias, J., Parés, C., 2001. A Q-scheme for a class of systems of coupled conservation laws with source term. Application to a two-layer 1D shallow water system. ESAIM Math. Model. Numer. Anal., 35, 1, 107–127.

Castro, M.J., Garcia-Rodriguez, J., González-Vida, J.M., Macas, J., Parés, C., Vázquez-Cendón, M., 2004. Numerical simulation of two-layer shallow water flows through channels with irregular geometry. J. Comput. Phys., 195, 1, 202–235.

Castro, M.J., Ferreiro Ferreiro, A., García-Rodríguez, J., González-Vida, J., Macas, J., Parés, C., Elena Vázquez-Cendón, M., 2005. The numerical treatment of wet/dry fronts in shallow flows: application to one-layer and two-layer systems. Math. Comput. Model., 42, 3–4, 419–439.

Castro, M.J., Gonzales-Vida, J., Pares, C., 2006. Numerical treatment of wet/dry fronts in shallow flows with a modified Roe scheme. Math. Models Methods Appl. Sci., 16, 6, 897–934.

Castro, M.J., García-Rodríguez, J.A., González-Vida, J.M., Macas, J., Parés, C., 2007. Improved FVM for two-layer shallow-water models: Application to the Strait of Gibraltar. Adv. Eng. Softw., 38, 6, 386–398.

Castro, M.J., Dumbser, M., Pares, C., Toro, E.F., 2009a. ADER schemes on unstructured meshes for nonconservative hyperbolic systems: applications to geophysical flows. Comp. & Fluids, 38, 1731–1748.

Castro, M.J., Fernández-Nieto, E.D., Ferreiro, A.M., García-Rodríguez, J.A., Parés, C., 2009b. High order extensions of Roe schemes for two-dimensional nonconservative hyperbolic systems. Journal of Scientific Computing, 39, 1, 67–114.

Castro, M.J., Fernandez-Nieto, E.D., Gonzalez-Vida, J.M., Pares, C., 2011. Numerical treatment of the loss of hyperbolicity of the two-layer shallow-water system. J. Sci. Comput., 48, 1, 16–40.

Dazzi, R., Tomasino, M., 1974. Mathematical model of salinity intrusion in the delta of the Po River. Coast. Eng. Proc., 134, 2302–2321.

Dermissis, V., Partheniades, E., 1985. Dominant shear stresses in arrested saline wedges. J. Waterw. Port, Coastal, Ocean Eng., 111, 4, 733–752.

Farmer, D., Armi, L., 1986. Maximal two-layer exchange over a sill and through the combination of a sill and contraction with barotropic flow. J. Fluid Mech., 164, 53–76.

Geyer, W.R., Ralston, D.K., 2011. The dynamics of strongly stratified estuaries. In: Wolanski, E., McLusky, D. (Eds.): Treatise on Estuarine and Coastal Science, Volume 2, Elsevier, pp. 37–52.

Grubert, J., 1989. Interfacial mixing in stratified channel flows. J. Hydraul. Eng., 115, 7, 887–905.

Hansen, D., Rattray Jr, M., 1966. New dimensions in estuary classification. Limnol. Oceanogr., 11, 3, 319–326.

Harten, A., 1984. On a class of high resolution total-variation-stable finite-difference schemes. SIAM J. Numer. Anal., 21, 1, 1–23.

Johnson, B., Boyd, M., Keulegan, G., 1987. A Mathematical Study of the Impact on Salinity Intrusion of Deepening the Lower Mississippi River Navigation Channel. Technical Report April, US Army Corps of Engineers, Vicksburg, Mississippi.

Krvavica, N., Mofardin, B., Ruzic, I., Ozanic, N., 2012. Measurement and analysis of salinization at the Rječina estuary. Gradevinar, 64, 11, 923–933.

Liu, H., Yoshikawa, N., Miyazu, S., Watanabe, K., 2015. Influence of saltwater wedges on irrigation water near a river estuary. Paddy Water Environ., 13, 2, 179–189.

Ljubenkov, I., 2015. Hydrodynamic modeling of stratified estuary: case study of the Jadro River (Croatia). J. Hydrol. Hydromech., 63, 1, 29–37.

Rebollo, T.C., Dom, A., Fern, E.D., 2003. A family of stable numerical solvers for the shallow water equations with source terms. Comput. Methods Appl. Mech. Eng., 192, 1–2, 203–225.

Roe, P., 1981. Approximate Riemann solvers, parameter vectors, and difference schemes. J. Comput. Phys., 43, 2, 357–372.

Sargent, F.E., Jirka, G.H., 1987. Experiments on saline wedge. J. Hydraul. Eng., 113, 10, 1307–1323.

Schijf, J., Schönfeld, J., 1953. Theoretical considerations on the motion of salt and fresh water. In: Proc. Minnesota Int. Hydraul. Conv., ASCE, Minneapolis, Minnesota, pp. 321–333.

Sierra, J.P., Sánchez-Arcilla, a., Figueras, P. a., González del Ro, J., Rassmussen, E.K., Mösso, C., 2004. Effects of discharge reductions on salt wedge dynamics of the Ebro River. River Res. Appl., 20, 1, 61–77.

Stommel, H.M., Farmer, H.G., 1952. On the nature of estuarine circulation, part 1, chap. 3 and 4. Technical report. Woods Hole Oceanographic Institution, Woods Hole, Massachusetts.

Vázquez-Cendón, M.E., 1999. Improved treatment of source terms in upwind schemes for the shallow water equations in channels with irregular geometry. J. Comput. Phys., 148, 2, 497–526.

Received 11 February 2016
Accepted 7 June 2016